

# Block Copolymer Crosslinked Nanoassemblies Co-entrapping Acridine Yellow and Doxorubicin for Cancer Theranostics

Pengxiao Cao, Andrei Ponta, JiAe Kim, Younsoo Bae\*

Department of Pharmaceutical Sciences, College of Pharmacy, University of Kentucky, 789  
South Limestone, Lexington, KY 40536, USA

## ABSTRACT

**Aims:** To develop block copolymer crosslinked nanoassemblies (CNAs) that co-entrap an imaging dye (Acridine Yellow: AY) and therapeutic agent (doxorubicin: DOX) as novel nanoparticle drug carriers for a combined application of drug delivery-based therapy and diagnostic imaging technologies (theranostics).

**Study design:** Physicochemical properties of AY-CNAs, such as molecular weight, particle size, surface charge, drug entrapment yield, and drug release profiles, were characterized prior to determining intracellular uptake profile, in vitro cytotoxicity, and in vivo tissue distribution patterns of the particles.

**Place and Duration of Study:** Department of Pharmaceutical Sciences (University of Kentucky), between June 2012 and January 2013.

**Methodology:** The AY-crosslinked CNAs (CNAs) were synthesized from biocompatible poly(ethylene glycol)-poly(aspartate) block copolymers by using AY as a crosslinker while DOX was physically entrapped in the particle through an ionic interaction. AY-CNAs and AY-CNAs with DOX were characterized to determine their particle properties (molecular weight, size, and optical properties), intracellular uptake and cytotoxicity in an in vitro cell culture system using human colon HT29 and lung A549 cancer cell lines, and tissue accumulation and tumor-preferential drug delivery efficiency ex vivo with a xenograft mouse tumor model.

**Results:** AY-CNAs appeared to maintain nanoscale particle sizes (< 20 nm), fluorescence optical properties, and negative surface charge before and after drug entrapment. AY-CNAs with DOX were confirmed to kill cancer cells as effectively as free drug formulations, and to enhance intracellular uptake in vitro and tumor accumulation ex vivo.

**Conclusion:** These results demonstrate that block copolymer nanoassemblies crosslinked with an imaging dye are promising platforms for the development of theranostic nanoparticle drug carriers.

**Keywords:** Nanoparticles, nanoassemblies, drug carriers, drug delivery, imaging, theranostics

## 1. INTRODUCTION

Nanoparticles have drawn attention as promising tools that can combine therapeutic and diagnostic modalities, which may allow doctors to monitor a progress of treatment and determine an optimal dose and timely intervention [1, 2]. Such a combination of therapy and diagnosis of disease, often known as theranostics, is particularly beneficial for treating

24 cancer patients who respond to chemotherapy differently [3, 4]. An optimal dose of an  
25 anticancer drug is typically determined by balancing chemotherapeutic efficacy and toxicity  
26 based on pharmacokinetic profiles of the drug [5, 6]. Nanoparticle drug carriers for  
27 theranostics are expected to expedite this dosing regimen determination process and  
28 provide novel cancer chemotherapy with enhanced efficacy and reduced toxicity [7, 8].

29 In recent years, various types of nanoparticles have been developed for cancer theranostics  
30 by conjugating imaging agents on the surface and entrapping therapeutic agents in the core  
31 [9, 10]. This approach is widely used for labeling proteins, RNAs, and DNA in biology, but  
32 often dramatically changes the particle properties of nanoparticles such as particle size,  
33 shape, surface charge, and interactions with live cells [11, 12]. One of the methods to avoid  
34 these undesirable particle property changes is to entrap imaging dyes in the core of  
35 nanoparticles [13]. However, entrapping imaging dyes into nanoparticles may lead to other  
36 issues such as fluorescence quenching, dye spectrum shifting, or reduced drug loading [14,  
37 15]. Therefore, developing a novel method that can entrap imaging agents in the  
38 nanoparticle core without altering particle properties is critically important for successful  
39 theranostics.

40 In addition to an imaging dye, a therapeutic agent is another payload to which careful  
41 consideration needs to be paid for the development of theranostic nanoparticles [16, 17].  
42 Drug molecules are generally entrapped in nanoparticles through either physical entrapment  
43 or chemical conjugation [18]. Although chemical drug conjugation via a degradable linker is  
44 advantageous to avoid uncontrolled release of drug from nanoparticle drug carriers, it  
45 frequently requires complicated chemistry for the synthesis of prodrugs and linkers [19-21].  
46 The chemical drug conjugation approach also requires validation if nanoparticles release the  
47 drug in its active form without forming byproduct during a linker degradation process. In this  
48 regard, physical drug entrapment is a more viable option to develop theranostic  
49 nanoparticles for combination delivery of imaging and therapeutic agents. Hydrophobic and  
50 ionic interactions are often used alone or in combination to entrap anticancer drugs inside  
51 nanoparticles. One of the model anticancer drugs used widely in drug delivery study is  
52 doxorubicin (DOX), an anthracycline agent that is effective to kill various types of cancer  
53 cells in the clinic [22]. The anthracycline portion of DOX is responsible for DNA intercalation  
54 and hydrophobic interaction with other molecules in the body while the amino group of DOX  
55 on the 4' position of the sugar can be used for ionic binding. DOX also has autofluorescence  
56 that can be easily monitored by UV-VIS and fluorescence spectrometry.

57 We have been developing biocompatible block copolymer crosslinked nanoassemblies  
58 (CNAs) for drug delivery and imaging [23, 24]. In this study, we used CNAs as molecular  
59 platforms to develop novel theranostic carriers for combination delivery of an imaging dye  
60 (Acridine Yellow: AY) and anticancer drug (DOX). As illustrated in Figure 1, AY was used as  
61 a crosslinker while DOX was entrapped in CNAs through an ionic interaction. The AY-  
62 crosslinked CNAs (AY-CNAs) were prepared from poly(ethylene glycol)-poly(aspartate)  
63 block copolymers that provide carboxyl groups for crosslinking and drug binding in the core  
64 enveloped by a hydrophilic shell. With this development approach, nanoparticles that co-  
65 entrap imaging and therapeutic agents can be prepared without any complicated chemical  
66 modification. The objective of this study is to characterize optical properties, intracellular  
67 uptake profile, and tissue accumulation patterns of AY-CNAs in vitro and ex vivo. These  
68 results are expected to provide valuable insights into the development of theranostic  
69 nanoparticles for cancer treatment by combining bioimaging and drug delivery technologies.

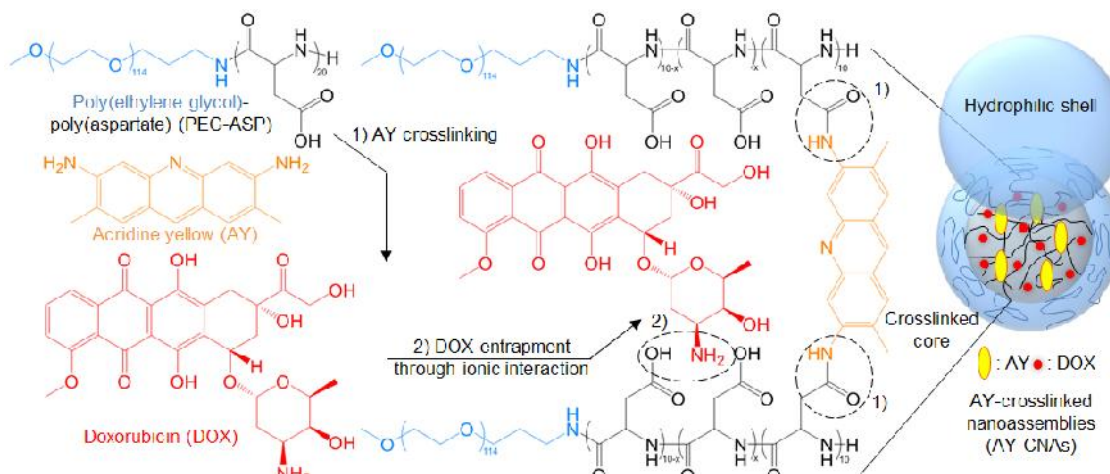


Fig. 1. Synthesis of AY-CNAs

70  
71  
72  
73  
74  
75  
76  
77  
78  
79  
80  
81  
82  
83  
84  
85  
86  
87  
88  
89  
90  
91  
92  
93  
94  
95  
96  
97  
98  
99  
100  
101  
102  
103  
104  
105  
106  
107

## 2. MATERIAL AND METHODS

### 2.1 Materials

NOF corporation (Japan) provided  $\alpha$ -methoxy- $\omega$ -amino poly(ethylene glycol) (PEG) (MW = 5,000). Doxorubicin hydrochloride (DOX-HCl), anhydrous triphosgene, L-aspartic acid  $\beta$ -benzyl ester, N,N'-diisopropylcarbodiimide (DIC), N-hydroxysuccinimide (NHS), 4-dimethylaminopyridine (DMAP), ethyl ether, dimethyl sulfoxide (DMSO), and other solvents were purchased from Sigma-Aldrich (USA). Acridine yellow (AY), cellulose dialysis bags with 6-8 kDa molecular weight cut off (MWCO), Slide-A-Lyzer dialysis cassettes with 10 kDa MWCO, sterile filters (0.22  $\mu$ m), and matrigel were purchased from Fisher Scientific (USA). Human colon (HT29) and lung (A549) cancer cell lines, and cell culture media (McCoy's 5A and F-12K) were purchased from ATCC (USA). Millicell EZ slide with 8 chambers were obtained from EMD Millipore (USA).

### 2.2 Synthesis of AY-CNAs

Figure 1 shows the synthesis protocol of AY-CNAs entrapping DOX. PEG-ASP was synthesized as described elsewhere [18, 25, 26]. L-aspartic acid  $\beta$ -benzyl ester was reacted with triphosgene to obtain  $\beta$ -benzyl aspartate N-carboxyanhydride (BLA-NCA) monomers. BLA-NCA was polymerized by using PEG as a macroinitiator for 2 days in DMSO (50 mg/mL, 40°C, nitrogen atmosphere). The polymerization produced PEG-poly( $\beta$ -benzyl L-aspartate) (PEG-BLA), comprising 5 kDa PEG and 20 repeating units of ASP groups. The benzyl ester protecting groups were removed in a 0.1 N NaOH solution to obtain PEG-ASP. Excess NaOH was removed from the polymer solution by dialysis, followed by freeze drying of PEG-ASP. The purified PEG-ASP was reacted with AY by adjusting the molar ratio between the aspartate groups of PEG-ASP and amino groups of AY (2:1) for a 50% crosslinking yield to balance the highest crosslinking yield with drug entrapment. PEG-ASP and AY were dissolved in DMSO in the presence of DIC, NHS, and DMAP for three days at room temperature with gentle stirring. The product, AY-CNAs, was precipitated in ethyl ether, dialyzed against deionized water, and collected by freeze drying. AY-CNAs were further purified by gel separation using a Sephadex G25 column, and unreacted AY was removed completely from AY-CNAs. A single band on the column containing AY-CNAs was collected, dialyzed against deionized water, and freeze dried. DOX was entrapped in AY-CNAs in deionized water through the ionic interaction between the amino group of DOX and

108 carboxyl groups of AY-CNAs, following the method previously reported [18]. Empty AY-  
109 CNAs and AY-CNAs with DOX were stored at -20°C for future use.

110

### 111 **2.3 Characterization of AY-CNAs**

112

113 The molecular weight and its distribution of AY-CNAs were analyzed by gel permeation  
114 chromatography (GPC), using Shimadzu LC20 system equipped with a GPC analysis  
115 module and a static light scattering detector for absolute molecular weight determination  
116 (Zetasizer  $\mu$ V, Malvern, UK). The particle size and surface charge of AY-CNAs and AY-  
117 CNAs with DOX were determined by a Zetasizer Nano ZS (Malvern, UK), an instrument  
118 capable of measuring dynamic light scattering (DLS) and zeta potential of nanoparticles in  
119 aqueous solutions. The amount of DOX entrapped in AY-CNAs was quantified by  
120 fluorescence spectrometry while empty AY-CNAs were used as blanks.

121

### 122 **2.4 Cellular uptake observations**

123

124 Time-dependent changes in cellular uptake of AY-CNAs were monitored in a human colon  
125 HT29 cancer cell line in vitro by using a fluorescence microscope (EVOS, Advanced  
126 Microscopy Group, USA). Cells were cultured in McCoy's 5A media containing 10% FBS at  
127 37°C in a humidified atmosphere with 5% CO<sub>2</sub>. For cellular uptake study, cells were seeded  
128 in 8 chamber slides ( $1 \times 10^4$  cells/chamber) and allowed to attach on the bottom of the slides  
129 overnight. The cells were then treated with 100  $\mu$ g/mL AY-CNAs for 24 h. The sample-  
130 containing media were removed at 5 min, 0.5 h, 3 h, and 24 h, and the cells were washed  
131 with PBS three times. Cell nuclei were stained with a Hoechst dye prior to fluorescence  
132 microscopy. Cell images were taken through separate light channels for a bright field,  
133 Hoechst, and AY, and processed using software ImageJ (National Institutes of Health, USA).  
134 In separate experiments, cells treated with AY-CNAs in each chamber were dissolved in  
135 80% DMSO, and the fluorescence intensity of AY-CNAs in the cell lysates were quantified by  
136 fluorescence spectrometry. The intracellular concentrations of AY-CNAs were normalized  
137 with respect to the initial concentration of AY-CNAs (100  $\mu$ g/mL) in each well. Data were  
138 obtained from triplicate experiments.

139

### 140 **2.5 Drug release evaluation**

141

142 Release of DOX from AY-CNAs was tested by the dialysis method under a sink condition at  
143 pH 7.4, 37°C. Ten milligrams of AY-CNAs with DOX were dissolved in 3 mL PBS, and the  
144 solution was put in dialysis cassettes (MWCO 10 kDa). The dialysis cassettes (n = 3) were  
145 stored in a preheated stainless steel bin containing 5 L PBS. The samples were dialyzed for  
146 48 h, and 50  $\mu$ L of the solution in each dialysis cassette was collected at 0.5, 1, 3, 6, 24, and  
147 48 h. DOX released was quantified by fluorescence spectrometry as described above.

148

### 149 **2.6 In vitro cytotoxicity assay**

150

151 Cytotoxicity of AY-CNAs with DOX was evaluated in an in vitro cell culture system by using  
152 HT29 and A549 cell lines. HT29 and A549 cells were cultured in McCoy's 5A and F12K  
153 media, respectively, containing 10% FBS at 37°C in a humidified atmosphere with 5% CO<sub>2</sub>.  
154 Cells were seeded in a 96 well plate ( $5 \times 10^3$  cells/well). After 24 h, the cells were treated  
155 with free DOX or AY-CNAs with DOX at various concentrations (normalized with respect to  
156 DOX). Empty AY-CNAs were used as controls. Cell viability was determined at 72 h post  
157 treatment by using a resazurin assay, which measures metabolic activity of mitochondria in  
158 live cells. The half maximal inhibitory concentration (IC<sub>50</sub>) of each sample was determined  
159 from the dose response curves by using GraphPad Prism software. The one-way analysis of  
160 variance (ANOVA) was used to determine statistical differences between means ( $p < 0.05$ ).

161 **2.7 Ex vivo imaging**

162

163 Six-week old female SCID mice were obtained from Taconic (USA), and acclimated for a  
164 week on a regular diet. A xenograft mouse tumor model was prepared by injecting HT29  
165 cells ( $3 \times 10^6$  cells) subcutaneously in the right flank of an animal. When the tumor volume  
166 surpassed  $100 \text{ mm}^3$ , AY-CNAs and AY-CNAs with DOX were injected into the tumor-bearing  
167 mice at  $100 \text{ mg/kg}$  through the tail vein. Animals were euthanized at 0.5, 2, 6, and 24 h post  
168 injections. Tumors and other major organs (lung, heart, liver, spleen, kidney, small intestine,  
169 and brain) were collected at each time point. An in vivo imaging system (IVIS) was used to  
170 take ex vivo images of the harvested tissues with excitation at 465 nm and emission at 540  
171 nm, based on the fluorescence spectra of free AY and DOX. The imaging condition was  
172 fixed to compare fluorescence intensities from the organ and tumor tissues.

173

174 **3. RESULTS**

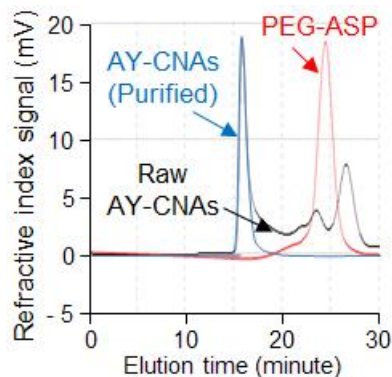
175

176 **3.1 Synthesis of AY-CNAs**

177

178 Gel permeation chromatography (GPC) analysis in Figure 2 shows the successful synthesis  
179 of AY-CNAs. The molecular weight of PEG-ASP (7,300 kDa) increased as the crosslinking  
180 reaction proceeded as shown in the black line. Raw AY-CNAs included small molecule  
181 impurities that appeared after the PEG-ASP peak at around 27 minutes. After purification,  
182 AY-CNAs showed a single peak with a narrow molecular weight distribution (262,500 kDa,  
183 PDI = 1.18), which was within the size exclusion limit of our GPC (970 - 478,000 kDa). The  
184 molecular weight of AY-CNAs indicates that a single CNA particle consists of 31 - 36 PEG-  
185 ASP chains depending on the crosslinking yield. Our attempt to determine the exact  
186 crosslinking yield was unsuccessful due to peak overlapping on proton nuclear magnetic  
187 resonance, and fluorescence spectrometry was used to quantify AY-CNAs by measuring AY.  
188 As shown in Figure 3, maximum emission wavelengths for AY and DOX were  
189 distinguishable by adjusting the excitation wavelength up to 500 nm. These optical  
190 properties of AY and DOX were initially thought to be useful quantifying a combine signal of  
191 AY and DOX. However, to avoid an overlapping signal between AY and DOX, we decided to  
192 used AY-CNAs and AY-CNAs with DOX for following experiments. Table 1 summarizes  
193 characterization data. The particle size of AY-CNAs was  $15.7 \pm 5.3 \text{ nm}$ , and the  
194 polydispersity index (PDI) was 0.384. The zeta potential of AY-CNAs was  $-14.7 \pm 9.8 \text{ mV}$ ,  
195 indicating that the particle may be too small for the PEG shell to completely shield the  
196 charge of the negatively charged core. The particle size of AY-CNAs was similar after  
197 entrapping DOX while the PDI went up to 0.418. The amount of DOX loaded in AY-CNAs  
198 was 4.65% by weight, which was significantly lower than other previous CNAs. The surface  
199 charge of AY-CNAs remained negatively charged ( $-10.2 \pm 6.2 \text{ mV}$ ) after entrapping DOX.

200



201

202

**Fig. 2. Gel permeation chromatography analysis**

203

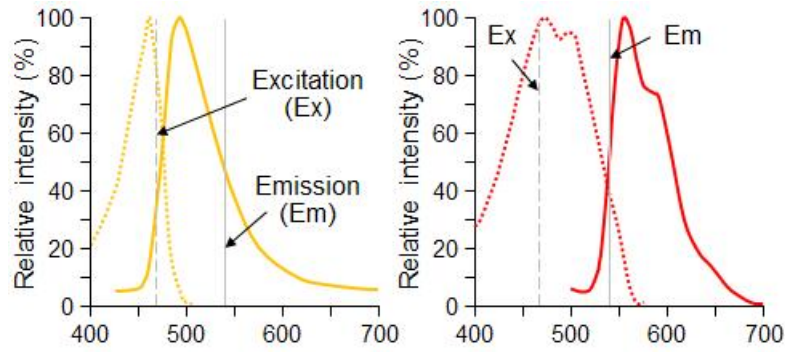


**Fig. 3. Fluorescence spectra of AY and DOX**

204  
205  
206  
207  
208

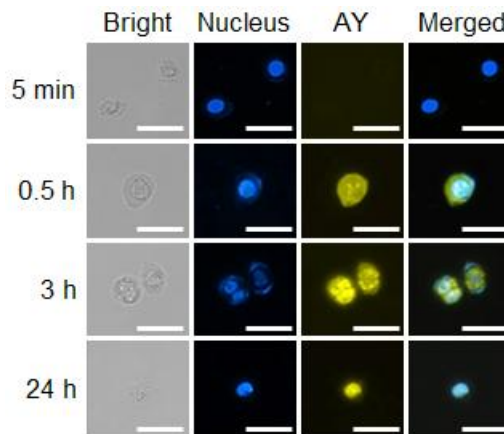
**Table 1. Characterization data summary**

	Particle size (nm)	PDI	Zeta potential (mV)	DOX loading (weight %)
AY-CNAs	15.69 ± 5.33	0.384	- 14.70 ± 9.78	N.A.
AY-CNAs with DOX	18.17 ± 5.98	0.418	- 10.20 ± 6.24	4.65

209  
210  
211  
212  
213  
214  
215  
216  
217  
218  
219  
220  
221  
222  
223

### 3.2 Intracellular uptake profile

Figure 4 shows time-dependent changes in intracellular uptake of AY-CNAs in HT29 cells. Non-specific binding to the cellular membrane was not observed between AY-CNAs and HT29 cells in 5 minutes. However, AY-CNAs entered and spread in the cytoplasm in 30 minutes. Interestingly, some AY-CNAs were confirmed to migrate into the cell nuclei as indicated in the merged image in green. No further change was observed after 24 h following a gradual increase in fluorescence intensity of AY-CNAs between 3 and 24 h. The intracellular concentration of AY-CNAs was also quantified from cell lysates in separate experiments. As shown in Figure 5, intracellular uptake of AY-CNAs followed biphasic kinetics, which involves a fast uptake in the early stage (up to 6 h) and a slow internalization into the cell in the late stage. The intracellular concentration of AY-CNAs did not equilibrate to the particle concentration in the media (100 µg/mL) under our experimental conditions.



224  
225  
226

**Fig. 4. Intracellular uptake of AY-CNAs. Bright field (40X magnification), Hoechst-stained nucleus (blue), AY (yellow), and merged images of HT29 cells (bar = 50 µm).**

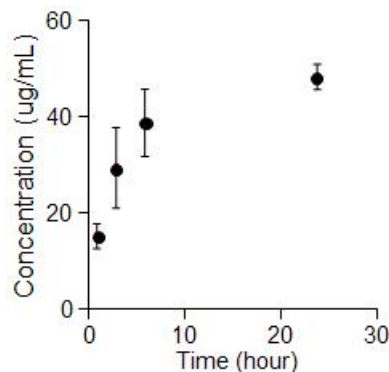


Fig. 5. A time-dependent change in concentration of AY-CNAs in HT29 cells.

228  
229  
230  
231  
232  
233  
234  
235  
236  
237  
238  
239  
240  
241  
242

### 3.3 Drug release patterns

Release of DOX was monitored for 48 h in the physiological condition (37°C and pH 7.4) as shown in Figure 6. AY-CNAs released more than 50% of DOX in 1 h, yet they slowed drug release for the next 48 h. Approximately 20% of total DOX entrapped in AY-CNAs was released between 3-48 h, although the drug release half-life was 1.34 h by curve fitting. Based on both intracellular uptake and drug release patterns, these results suggest that the amount of DOX that AY-CNAs can transport inside the HT29 cells would be approximately 12 - 17 % (= DOX remaining × intracellular uptake yield) over the 48 h period. The effect of such a fast drug release and relatively low intracellular drug transport on anticancer efficacy was investigated subsequently in the cytotoxicity assays.

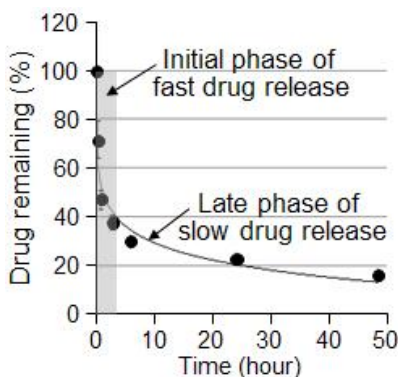


Fig. 6. Biphasic DOX release from AY-CNAs (pH 7.4, 37°C, n = 3)

243  
244  
245  
246  
247  
248  
249  
250  
251  
252  
253  
254  
255  
256  
257

### 3.4 In vitro cytotoxicity of AY-CNAs with DOX

Cytotoxicity of AY-CNAs with DOX was evaluated in exponentially growing HT29 cells in vitro. A549 was used as an additional cancer cell line for the assay. As shown in Figure 7, sigmoidal dose-response curves were obtained from both cancer cell lines, following the treatment of the cells with AY-CNAs entrapping DOX. Table 2 summarizes the IC<sub>50</sub> values of AY-CNAs, which range between 3.03 - 4.80 μM. Although relative IC<sub>50</sub> values suggested that AY-CNAs with DOX would be less potent than free DOX, statistical analysis of the data revealed that both cell lines were equally sensitive to free DOX (p = 0.240) and AY-CNAs with DOX (p = 0.051). Considering the slow drug release from AY-CNAs after 3 h post incubation, it is noticeable that free DOX and AY-CNAs with DOX showed no significant difference in killing HT29 (p = 0.224) and A549 (p = 0.654) cancer cells.

258

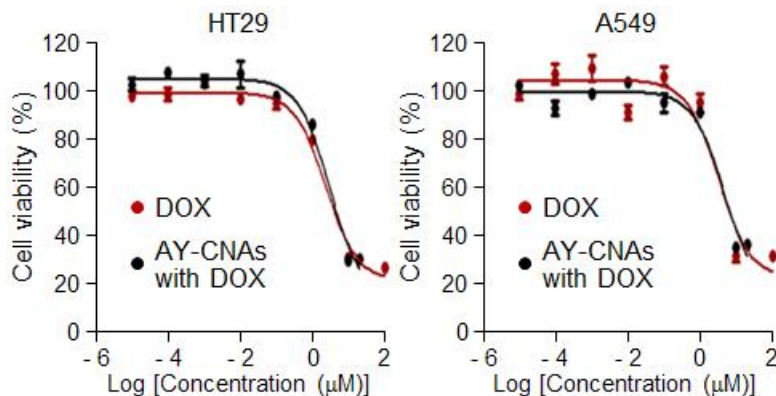


Fig. 7. Cytotoxicity of AY-CNAs against HT29 and A549 cells (triplicate assays, n = 8)

259  
260  
261  
262  
263

Table 2. In vitro cytotoxicity assays (triplicate assays, n = 8)

	IC50 (μM)		Relative IC50	
	HT29	A549	HT29	A549
DOX	2.44 ± 0.65	3.08 ± 0.47	1	1
AY-CNAs with DOX	3.03 ± 0.27	4.80 ± 1.09	1.56	1.24

264  
265

### 3.5 Tissue distribution of AY-CNAs with DOX

266  
267  
268  
269  
270  
271  
272  
273  
274  
275  
276  
277  
278  
279  
280

Tissue accumulation patterns of AY-CNAs were investigated time-dependently as shown in Figure 8. The images were taken under the condition where AY and DOX showed equal fluorescence emission intensity at 540 nm with excitation at 465 nm as determined in Figure 3. In this way, signals from AY and DOX were obtained collectively. AY-CNAs appeared to accumulate in the kidneys, intestine, and tumors, while avoiding the uptake in the liver and spleen. The liver and spleen are two major organs of the mononuclear phagocyte system (MPS), which are responsible for removing foreign materials from the body. **These results suggest that negatively charged AY-CNAs could be effective to suppress protein adsorption and cellular interactions in the body [12]. Although detailed mechanisms need to be studied further, enhanced accumulation of AY-CNAs in kidneys may be attributed to the relatively small particle size (< 20 nm).** AY-CNAs with DOX also suppressed the hepatic and splenic uptake while accumulating in tumors. The images demonstrate that AY-CNAs with DOX increased signals in tumors in comparison to empty AY-CNAs presumably due to enhanced DOX accumulation in the tumors.

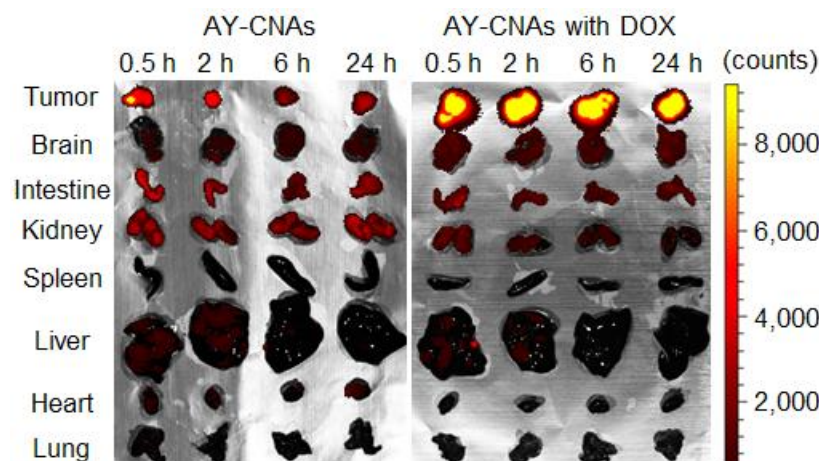
281  
282

## 4. DISCUSSION

283  
284  
285  
286  
287  
288  
289  
290  
291  
292

AY-CNAs were synthesized by using AY as a crosslinker for conjugating PEG-ASP block copolymers. AY is also a fluorescent dye useful for in vitro and ex vivo imaging [27]. Nanoparticles for imaging are typically modified with fluorescent dyes on the surface. This modification method often alters particle properties of the nanoparticles, such as particle size, surface charge, biocompatibility, and pharmacokinetic profiles [28]. In comparison to this method, our approach to use a fluorescent dye as a crosslinker does not require additional chemical modification of a nanoparticle, and thus maintaining particle properties for optimal in vivo performance (prolonged blood circulation and minimum off-target accumulation).





293  
294 **Fig. 8. Ex vivo imaging of tumors and major organs from mice received intravenously**  
295 **AY-CNAs and AY-CNAs with DOX.**  
296

297  
298  
299  
300  
301  
302  
303  
304  
305  
306  
307  
308  
309  
310  
311  
 AY-CNAs were uniform in terms of molecular weight distribution as shown in Table 1 and Figure 2. However, the particle size was relatively small (< 20 nm) as opposed to the CNAs we reported previously or other types of nanoparticles (50 - 100 nm in diameter) [22-24]. The small particle size suggested that the core of AY-CNAs could be tightly packed. Nanoparticles with a tightly packed core often induced a fluorescence quenching phenomenon, but AY-CNAs retained optical properties of AY and DOX as shown in Figures 3 and 4. Therefore, it is surmised that there is still enough space for AY or DOX molecules to move in 20 nm CNAs and avoid fluorescence quenching. Small particle size indeed compromised drug loading efficiency for the particles, and AY-CNAs showed less than 5 wt% of drug loading. Nevertheless, AY-CNAs with a small particle size seemed to enhance intracellular uptake of cancer cells. The particles successfully entered HT29 cancer cells as early as 30 minutes, and continue to accumulate in the cytoplasm and ultimately in the cell nucleus in 24 h (Figures 4 and 5). Such an efficient cell internalization pattern suggests that AY-CNAs would be a promising drug carrier for intracellular drug delivery. The mechanism by which AY-CNAs enter the cell certainly requires further study [29, 30].

312  
313  
314  
315  
316  
317  
318  
319  
320  
321  
322  
323  
324  
325  
326  
327  
328  
 Despite the promising properties (uniform particles with a small size and enhanced cell internalization capability), AY-CNAs released drug unexpectedly fast (Figure 6), demonstrating burst DOX release in 3 h and sustained release for the next 48 h. It is uncertain if such a biphasic drug release pattern would provide any benefit in terms of enhancing antitumor activity. Interestingly, fast release (or sustained release) did not affect cytotoxicity of AY-CNAs with DOX in an in vitro cell culture system. Both HT29 and A549 cells were sensitive to AY-CNAs with DOX, which were as effective as free DOX in terms of IC50 values (Figure 7). Ex vivo imaging suggest that sustained drug release from AY-CNAs in the late stage would still allow the particles to deliver drug to tumors and enhance drug concentrations in the tumor tissues preferentially, suppressing off-target drug distribution (Figure 8). It must be noted that AY-CNAs with a small particle size were confirmed to accumulate mainly in kidneys and intestine other than tumors. Pathological similarities among kidneys, intestine, and tumors have not been studied sufficiently yet, and the reason behind our findings remains uncertain. However, it is encouraging that AY-CNAs can be present in these tissues after 24 h, which might lead to the development of drug delivery systems for novel therapeutic or diagnostic applications.

329 **5. CONCLUSION**

330

331

332

333

334

335

336

337

338

339

340

341

342

343

344

345

346

347

348

349

In this study, AY-CNAs, block copolymer nanoassemblies crosslinked by a fluorescent dye, were synthesized for potential combination delivery of imaging and therapeutic agents to tumors. AY-CNAs were uniform in size and molecular weight distribution while maintaining negative surface charge before and after entrapping DOX, a model anticancer drug. Optical properties of AY and DOX were comparable yet different enough to distinguish, enabling both additive and differential quantifications of fluorescence emission signals at the same excitation wavelength. AY-CNAs entered cancer cells in 30 minutes post-incubation, and ultimately accumulated in cell nuclei in 24 h, presumably due to their small particle size (< 20 nm). AY-CNAs entrapping DOX released approximately 60% of the total drug entrapped in 3 h, and showed a sustained release of the remaining drug over the 48 period. Despite the biphasic drug release pattern, AY-CNAs with DOX showed cytotoxicity as effective as free DOX against human colon HT29 and lung A549 cancer cells in vitro. Ex vivo imaging results confirmed that AY-CNAs and AY-CNAs with DOX accumulate mainly in tumors and kidneys while suppressing hepatic and splenic uptake. Taken together, AY-CNAs are expected to be used as dual functional nanoscale carriers for bioimaging and drug delivery applications.

**ACKNOWLEDGEMENTS**

This research is supported by the Kentucky Lung Cancer Research Program.

350  
351  
352  
353  
354  
355  
356  
357  
358  
359  
360  
361  
362  
363  
364  
365  
366  
367  
368  
369  
370  
371  
372  
373  
374  
375  
376  
377  
378  
379  
380  
381  
382  
383  
384  
385  
386  
387  
388  
389  
390  
391  
392  
393  
394  
395  
396  
397  
398  
399  
400  
401

## REFERENCES

1. Lammers T, Aime S, Hennink WE, Storm G, Kiessling F. Theranostic nanomedicine. *Acc Chem Res.* 2011;44(10):1029-1038.
2. Chen W, Xu NF, Xu LG, Wang LB, Li ZK, Ma W, et al. Multifunctional Magnetoplasmonic Nanoparticle Assemblies for Cancer Therapy and Diagnostics (Theranostics). *Macromol Rapid Comm.* 2010;31(2):228-236.
3. Janib SM, Moses AS, MacKay JA. Imaging and drug delivery using theranostic nanoparticles. *Adv Drug Deliver Rev.* 2010;62(11):1052-1063.
4. Parveen S, Misra R, Sahoo SK. Nanoparticles: a boon to drug delivery, therapeutics, diagnostics and imaging. *Nanomed-Nanotechnol.* 2012;8(2):147-166.
5. Baselga J, Mita AC, Schoffski P, Dumez H, Rojo F, Tabernero J, et al. Using Pharmacokinetic and Pharmacodynamic Data in Early Decision Making Regarding Drug Development: A Phase I Clinical Trial Evaluating Tyrosine Kinase Inhibitor, AEE788. *Clin Cancer Res.* 2012;18(22):6364-6372.
6. Pagano A, Honore S, Esteve MA, Braguer D. Nanodrug potential in cancer therapy: efficacy/toxicity studies in cancer cells. *Int J Nanotechnol.* 2012;9(3-7):502-516.
7. Saif MW, Choma A, Salamone SJ, Chu E. Pharmacokinetically Guided Dose Adjustment of 5-Fluorouracil: A Rational Approach to Improving Therapeutic Outcomes. *J Natl Cancer I.* 2009;101(22):1543-1552.
8. Kopecek J. Biomaterials and Drug Delivery: Past, Present, and Future. *Mol Pharm.* 2010;7(4):922-925.
9. Xie J, Lee S, Chen XY. Nanoparticle-based theranostic agents. *Adv Drug Deliver Rev.* 2010;62(11):1064-1079.
10. Adair JH, Parette MP, Altinoglu EI, Kester M. Nanoparticulate Alternatives for Drug Delivery. *Acs Nano.* 2010;4(9):4967-4970.
11. Rosenblum LT, Kosaka N, Mitsunaga M, Choyke PL, Kobayashi H. In vivo molecular imaging using nanomaterials: General in vivo characteristics of nano-sized reagents and applications for cancer diagnosis (Review). *Mol Membr Biol.* 2010;27(7):274-285.
12. He CB, Hu YP, Yin LC, Tang C, Yin CH. Effects of particle size and surface charge on cellular uptake and biodistribution of polymeric nanoparticles. *Biomaterials.* 2010;31(13):3657-3666.
13. Cormode DP, Skajaa T, Fayad ZA, Mulder WJM. Nanotechnology in Medical Imaging Probe Design and Applications. *Arterioscl Throm Vas.* 2009;29(7):992-1000.
14. Louie AY. Multimodality Imaging Probes: Design and Challenges. *Chem Rev.* 2010;110(5):3146-3195.
15. Gao JH, Chen K, Luong R, Bouley DM, Mao H, Qiao TC, et al. A Novel Clinically Translatable Fluorescent Nanoparticle for Targeted Molecular Imaging of Tumors in Living Subjects. *Nano Lett.* 2012;12(1):281-286.
16. Yap TA, Sandhu SK, Workman P, de Bono JS. Envisioning the future of early anticancer drug development. *Nat Rev Cancer.* 2010;10(7):514-U525.
17. Rask-Andersen M, Almen MS, Schioth HB. Trends in the exploitation of novel drug targets. *Nat Rev Drug Discov.* 2011;10(8):579-590.
18. Lee HJ, Bae Y. Pharmaceutical Differences Between Block Copolymer Self-Assembled and Cross-Linked Nanoassemblies as Carriers for Tunable Drug Release. *Pharm Res.* 2013;30(2):478-488.
19. Larson N, Ghandehari H. Polymeric Conjugates for Drug Delivery. *Chem Mater.* 2012;24(5):840-853.
20. Binauld S, Stenzel MH. Acid-degradable polymers for drug delivery: a decade of innovation. *Chem Commun.* 2013;49(21):2082-2102.
21. Wanakule P, Roy K. Disease-Responsive Drug Delivery: The Next Generation of Smart Delivery Devices. *Curr Drug Metab.* 2012;13(1):42-49.

- 402 22. Bae Y, Kataoka K. Intelligent polymeric micelles from functional poly(ethylene glycol)-  
403 poly(amino acid) block copolymers. *Adv Drug Deliver Rev.* 2009;61(10):768-784.
- 404 23. Lee HJ, Bae Y. Cross-Linked Nanoassemblies from Poly(ethylene glycol)-poly(aspartate)  
405 Block Copolymers as Stable Supramolecular Templates for Particulate Drug Delivery.  
406 *Biomacromolecules.* 2011;12(7):2686-2696.
- 407 24. Lee HJ, Ponta A, Bae Y. Polymer nanoassemblies for cancer treatment and imaging.  
408 *Ther Deliv.* 2010;1(6):803-817.
- 409 25. Bae Y, Jang W-D, Nishiyama N, Fukushima S, Kataoka K. Multifunctional polymeric  
410 micelles with folate-mediated cancer cell targeting and pH-triggered drug releasing  
411 properties for active intracellular drug delivery. *Mol BioSyst.* 2005;1(3):242-250.
- 412 26. Bae Y, Fukushima S, Harada A, Kataoka K. Design of environment-sensitive  
413 supramolecular assemblies for intracellular drug delivery: Polymeric micelles that are  
414 responsive to intracellular pH change. *Angew Chem Int Ed.* 2003;42(38):4640-4643.
- 415 27. Mahmood T, Wu Y, Loriot D, Kuimova M, Ladame S. Closing the ring to bring up the  
416 light: synthesis of a hexacyclic acridinium cyanine dye. *Chemistry.* 2012;18(39):12349-  
417 12356.
- 418 28. Cho EC, Au L, Zhang Q, Xia YN. The Effects of Size, Shape, and Surface Functional  
419 Group of Gold Nanostructures on Their Adsorption and Internalization by Cells. *Small.*  
420 2010;6(4):517-522.
- 421 29. Yoo JW, Doshi N, Mitragotri S. Endocytosis and Intracellular Distribution of PLGA  
422 Particles in Endothelial Cells: Effect of Particle Geometry. *Macromol Rapid Comm.*  
423 2010;31(2):142-148.
- 424 30. Misra R, Sahoo SK. Intracellular trafficking of nuclear localization signal conjugated  
425 nanoparticles for cancer therapy. *Eur J Pharm Sci.* 2010;39(1-3):152-163.